Colloid Polym Sci 274:741–746 (1996)

ORIGINAL CONTRIBUTION

Studies on styrene phosphonic acid

P.C. Schulz
B.S. Fernández-Band
B. Vuano
M. Palomeque
A.L. Allan

Received: 25 July 1995
Accepted: 23 December 1995

Dr. P.C. Schulz (✉) · B.S. Fernández-Band
B. Vuano · M. Palomeque · A.L. Allan
Department of Chemistry and Chemical Engineering
Universidad Nacional del Sur
8000 Bahia Blanca, Argentina

Abstract Some properties of styrene phosphonic acid (SPA) were studied. The crystals were triclinic, with $a = 0.6434$ nm, $b = 0.5842$ nm, $c = 2.0338$ nm, $\alpha = 96.17°$, $\beta = 97.33°$, $\gamma = 79.65°$ and $Z = 4$. SPA underwent a change in crystal structure at 78.8 °C, the hydrocarbon network became disordered ("liquid-like") at 138.5 °C. Crystals melted at 148.6 °C giving a cubic mesophase, then changed to an isotropic liquid at 155.6 °C and at 162.13 °C SPA underwent decomposition. Values for $pK_1 = 2.15$ and $pK_2 = 7.66$ were obtained at 25 °C. The water solubility of SPA at several temperatures, and its interaction with surfactant micelles were determined.

Key words Styrene phosphonic acid – crystals – micelle solubilization – solubility

Introduction

Styrene phosphonic acid (SPA) has industrial applications in ore flotation [1–3], where the SPA is used as a collector in cassiterite flotation for tin concentrators [4], in ion extraction, in chelation [5–9], in polymer manufacture [10], as an additive in the paper industry [11], and as a corrosion scale inhibitor [12] etc. SPA interactions with micelles are important in some of the above mentioned applications.

Experimental

SPA (C_6H_5–CH = CH–PO_3H_2) was synthesized according to a literature method [13].

Differential scanning calorimetry (DSC) studies were performed with a Perkin Elmer DSC-4 differential calorimeter, with an Intracooler I refrigeration unit. The runs were carried out in aluminum pans at 10 °C/min. The instrument was calibrated with an indium standard. All determinations were performed in a nitrogen flow.

Microscopic observations were performed in a Leitz polarized light microscope with a Chaixmeca temperature-controlled stage.

X-ray diffractograms were obtained with a Rigaku Denki instrument controlled with a computer, using CuKα radiation and nickel filter. The diffragtograms were analyzed according to the Vand method [14, 15].

The SPA solution density was measured with a 25 mL pycnometer, using a saturated SPA aqueous solution as filling liquid. The density of this solution was 1001.6 ± 0.2 kg/m^3 at 25 °C (average of five determinations).

The acidity constants were determined titrimetrically at three different temperatures (25° – 30° – 40 °C) using an AMEL 234 automatic titrator and a digital burette model 233. The titrations were carried out in a nitrogen atmosphere to avoid CO_2 effects. The standard solution used was 8.44×10^{-2} M NaOH. An ionic strength of 0.1 mol/L was maintained by adding $KClO_4$.

pK_1 and pK_2 values were corrected using activity coefficients obtained by the Davies equation (16)

$$\log \gamma_i = |Z_i^2| \left[-\frac{A\sqrt{I}}{1+\sqrt{I}} + 0.15I \right], \qquad (1)$$

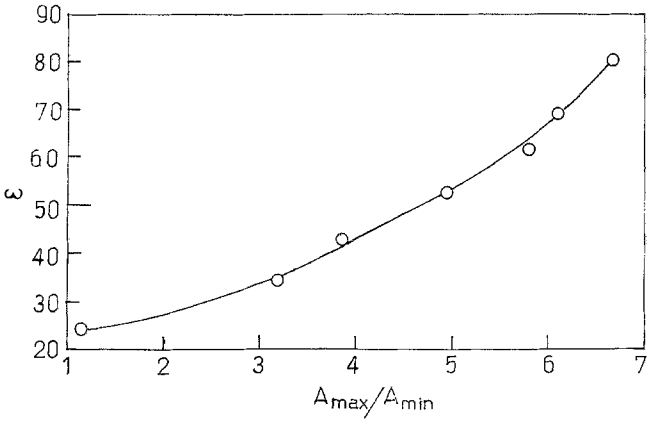

Fig. 1 Solvent dielectric constant vs. A_{max}/A_{min} for SPA

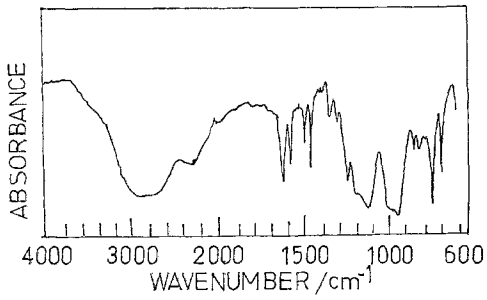

Fig. 2 IR spectrum of solid SPA in KBr

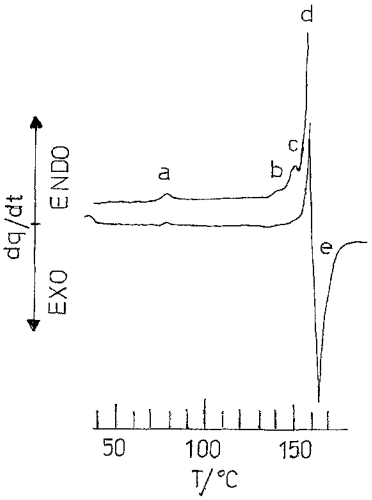

Fig. 3 DSC thermogram of pure SPA

where I is the ionic strength, and Z_i and γ_i the valence and the activity coefficient of the ion i. The A values were computed for each temperature.

The solubility measurements were performed by thermostatting for 2 h using water containing an excess of solid SPA, with periodic shaking. After sedimentation, the supernatant liquid was separated and placed in a weighed container and dried until a constant weight was obtained. Four determinations were made at each temperature. The absence of water was verified by IR spectroscopy.

The UV-visible spectra of 7.60×10^{-5} M SPA in different solvents (water, and using 0.016 M dodecyltrimethylammonium bromide (DTAB), were determined using a Shimadzu UV 160 spectrophotometer. The dielectric constant (ε) of the SPA microenvironment was investigated by the dependence of the A_{max}/A_{min} ratio with the solvent value of ε [17], A_{max} and A_{min} being the absorbances at the maximum (≈ 255 nm) and the adjacent minimum (≈ 245 nm). The surfactant spectrum was subtracted to compute this ratio. The calibration curve (Fig. 1) was obtained using aqueous methyl alcohol solutions of known ε values [18].

The confidence intervals were computed with Student's t function at a confidence level of 0.90. Linear regressions and averages were computed by an unbiased linear least variance method [19].

Results

The SPA IR spectrum (Fig. 2) shows that there was no water of crystallization. The P=O groups are associated to the −OH groups by hydrogen bonds, as in other phosphonic acids crystals [20–22].

The density of SPA was 1625 ± 6 kg/m^3 at 25 °C.

DSC thermograms (Fig. 3) have shown the following transitions: a) at 78.8 ± 1.0 °C, with an associated enthalpy $\Delta H_a = 689 \pm 6$ J/mol; b) at 138.5 ± 1.5 °C, with $\Delta H_b = 1.45 \pm 0.24$ kJ/mol; c) at 148.8 ± 1.9 °C with $\Delta H_c = 2.02 \pm 0.18$ kJ/mol; d) at 155.6 ± 1.0 °C with $\Delta H_d = 13.5 \pm 0.7$ kJ/mol; and e) at 162.13 ± 0.31 °C with $\Delta H_e = -47.7 \pm 1.1$ kJ/mol.

The microscopic observation with polarized light at low temperature showed weakly birefringent lamellar crystals (Fig. 4) with diagonal fractures, showing interference colors. The microscopically measured angles between edges were 97.62° (β), 77.37° (γ) and 60.7° (between the (010) and (210) planes). Crystals showed the (010) and (001) faces, and an oblique extinction, almost parallel to the "c" axis.

No changes in optical texture were seen at transition a). The crystals became opaque with waxy texture at transition b). This was associated in other phosphonic acid crystals with the transition to a "liquid-like" state of the hydrocarbon network [20, 21]. Crystals melted to a non-birefringent, viscous liquid at transition c). No texture changes were seen at d). Transition d) coincided with the determination of the SPA melting point using a heated

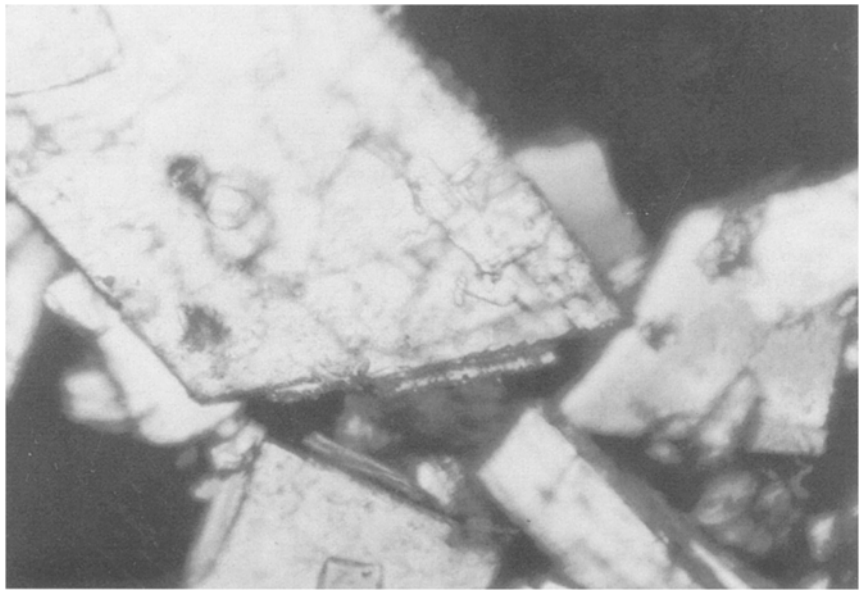

Fig. 4 SPA crystals, crossed polaroids, X60

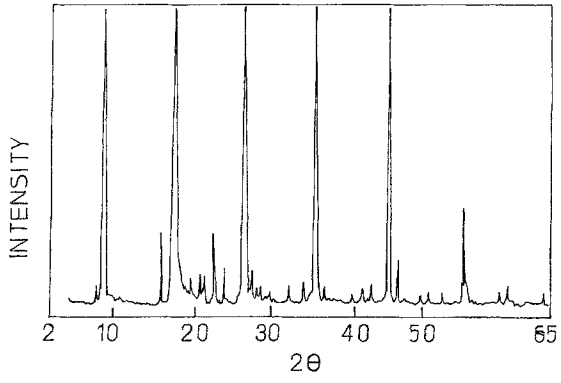

Fig. 5 X-ray diffractogram of SPA crystals at room temperature

stage Köffler microscope (155–157 °C). The sample disappeared at transition e). When this DSC exothermic peak was reached, the cooling thermogram did not show any transition.

Figure 5 shows the x-ray diffractogram of the low temperature crystal phase. Table 1 shows H^*_{hk} and L^*_{hkl} values, which were obtained from the diffractogram according to the Vand method [14, 15]. These values were related to the crystalline reciprocal network parameters (labelled with *) by:

$$H^*_{hk} = h^2A^{*2} + h^2B^{*2} - 2hkA^*B^* \cos\gamma \tag{2}$$

$$L^*_{hkl} = lc^* + hA^* \cot\beta^* + kB^* \cot\alpha^* , \tag{3}$$

where

$$A^* = a^* \sin\beta^* \quad \text{and} \quad B^* = b^* \sin\alpha^* . \tag{4}$$

Table 1 Values of H^*_{hk} and L^*_{hkl} obtained from the SPA X-ray diffractogram

h	k	l	H^*_{hk}	L^*_{hkl}
1	0	0	0.158	0.027
0	1	0	0.174	0.014
1	1		0.213	
2	0		0.213	
1	2		0.236	
3	0		0.2535	
1	3		0.260	
2	1		0.266	

The crystalline reciprocal network parameters were related to the parameters of the elementary cell as follows:

$$a = \frac{1}{A^* \sin\gamma} \qquad b = \frac{1}{B^* \sin\gamma} \tag{5}$$

$$\cos\gamma^* = \cos\alpha^* \cdot \cos\beta^* - \sin\alpha^* \cdot \sin\beta^* \cdot \cos\gamma \tag{6}$$

$$\cos\alpha = \frac{\cos\beta^* \cdot \cos\gamma^* - \cos\alpha^*}{\sin\beta^* \cdot \sin\gamma^*} \tag{7}$$

$$\cos\beta = \frac{\cos\alpha^* \cdot \cos\gamma^* - \cos\beta^*}{\sin\beta^* \cdot \sin\gamma^*} \tag{7}$$

$$c = \frac{1}{c^* \cdot \sin\beta \cdot \sin\alpha^*} \tag{8}$$

The pK_1 and pK_2 values obtained at different values are shown in Table 2, and the SPA water solubilities at different temperatures are shown in Table 3.

Table 2 pK_1 and pK_2 of SPA in water at different temperatures

T (°C)	pK_1	pK_2
25	2.15 ± 0.09	7.66 ± 0.03
30	2.02 ± 0.06	7.62 ± 0.03
40	2.17 ± 0.04	7.61 ± 0.03

Table 3 Water solubility of SPA at different temperatures

T (°C)	Solubility (g/100 mL)
25	1.906 ± 0.008
35	2.280 ± 0.007
47	2.813 ± 0.005
55	3.209 ± 0.009

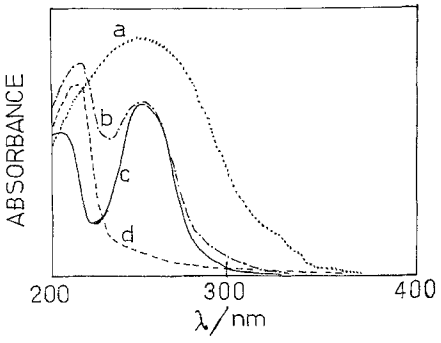

Fig. 6 UV-Vis spectra of SPA in: a) absolute ethanol, b) aqueous DTAB, c) water, d) pure DTAB spectrum in water

Figure 6 shows the UV-Vis spectra of SPA in different solvents, water, absolute ethyl alcohol and aqueous dodecyltrimethylammonium bromide (DTAB), and the spectrum of DTAB in water. The non-aromatic $\pi \rightarrow \pi^*$ band was shifted from 255 to 250 nm and it is increased from the spectrum in water to that in aqueous DTAB. This weak band overlapped the benzene band at 260 nm, and is slightly intensified by polar substitution.

The $\pi \rightarrow \pi^*$ aromatic band at 207 nm shifted to below 200 nm and thus is out of the spectrum range of the instrument. This is due to the polarity change in the microenvironment of the SPA molecules. The band at 217 nm is assumed to belong to DTAB.

Similar changes were seen in the spectrum of SPA dissolved in aqueous sodium dodecylsulphate (SDS).

Discussion

Structure and thermal behavior

The low-temperature SPA elementary cell was triclinic with $a = 0.643$ nm, $b = 0.5842$ nm, $c = 2.0338$ nm, $\alpha = 96.17°$, $\beta = 97.33°$ and $\gamma = 79.65°$. In agreement with the density, the number of molecules in the elementary cell (Z) is 4. By comparison of elementary cell dimensions with those of the SPA molecule, and by analogy with other phosphonate crystalline structures [21], the disposition of the SPA molecules in the elementary cell shown in Fig. 7 is proposed. SPA molecules are arranged in double polar layers between double apolar layers, as in crystals of other amphiphilic molecules. The polar groups are above the (001) plane. The molecular plane of the aromatic ring is parallel to the (010) plane. The area covered by the polar groups is 1.86 nm^2 on the (001) plane, which is comparable to that of other phosphonic acids [20]. The crystallographic density is1627 kg/m^3.

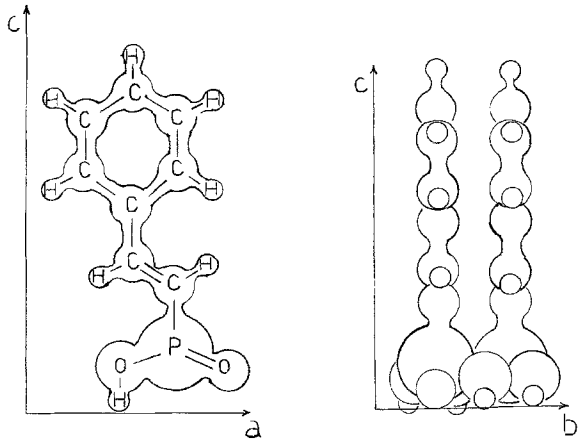

Fig. 7 Proposed disposition of the SPA molecules in the elementary cell. The "a" and "b" axis are in the (001) plane

The transition a) which occurs at 78.8 ± 1.0 °C, with a low enthalpy change (689 ± 6 J/mol) is probably due to a slight change in crystalline structure, and is undetectable by microscopical observation.

The transition b) to a "waxy" texture is comparable to the transition observed in other substances which have similar crystalline structures i.e., an imbrication of polar and non-polar layers: the non-polar layer "melted" to a disordered, liquid-like state [21, 23]. Above this transition the double styrene layers became liquid-like, while the polar layer remained almost intact, with a slight alternation of hydrogen bonds [20].

The transition c) (at 148.6 ± 1.9 °C) corresponds to the melting of the crystals giving a cubic (viscoisotropic) mesophase, which was transformed to an unorganized, isotropic liquid at transition d) (155.6 ± 1.0 °C).

At transition e) (162.13 ± 0.31 °C) the isotropic liquid decomposes exothermically.

Transitions a), b) and c) are close to each other owing to steric factors. On account of the non-polar groups size, the polar group arrangement cannot be very compact. Its

cohesion is thus weak, yielding easily to the transition between rigid and dynamic hydrogen bonds (transition c)).

Ionization

The values of pK_1 and pK_2 (2.15 and 7.66 at 25 °C) suggest that the SPA ionization is slighty lower than those compounds whose $-PO_3H_2$ groups are bound to an aromatic ring ($pK_1 = 1.83$ and $pK_2 = 7.07$ for benzene phosphonic acid); and still lower pK values are found for subsituted benzene phosphonic acids [24].

The pK_1 value is lower than that of alkylphosphonic acids ($pK_1 = 3.976 \pm 0.001$ for *n*-decanephosphonic acid [25]), while pK_2 is not very different from the abovementioned compound ($pK_2 = 7.985 \pm 0.003$ for *n*-decanephosphonic acid [25]). The same effect was seen for other aromatic phosphonic acids [24].

It may be concluded that the first ionization process is affected by a delocalization of a negative charge over the π system, stabilizing the monoionized anion; while the second ionization is affected by the electrostatic attraction between the H^+ ion and the double-charged anion, whose second negative charge is located over an oxygen atom.

pK_1 and pK_2 values are altered in different solvents. So, SPA in 18% V/V dimethylformamide – water solution showed $pK_1 = 5.64$ and $pK_2 = 10.4$ at 25 °C [26]. A similar effect was seen with aromatic phosphonic acids in aqueous alcoholic solutions, e.g., $pK_1 = 3.15$ and $pK_2 = 8.26$ for benzene phosphonic acid in 50% ethanol–water solution [24].

The values of pK_1 and pK_2 were invariable with temperature (Table 2). This means that the dissociation process is fundamentally entropic ($\Delta H_{diss.} \approx 0$):

$$\Delta G_{diss.} = -RT \ln K_a = \Delta H_{diss.} - T\Delta S_{diss.} \approx -T\Delta S_{diss.} \quad (10)$$

The dissociation entropies were computed from the pK values, and the average values are $\Delta S_1 = -7.73 \pm 0.26\ JK^{-1}mol^{-1}$ and $\Delta S_2 = -27.54 \pm 0.14\ JK^{-1}mol^{-1}$. The low absolute value of ΔS_1 is due to the loss of freedom of the water molecules bound to the hydronium ions, and to formation of the monocharged styrene phosphonic group whose negative charge is spread over the π system. The ΔS_2 value is higher due to a stronger interaction of water molecules with the localized negative charge on the oxygen atoms.

Interaction with micelles

The SPA spectra in different solvents showed a weak shift of the maximum position, but the A_{max}/A_{min} ratio showed a well-defined dependence with the solvent dielectric constant (ε), shown in Fig. 1. The A_{max}/A_{min} ratio was 1.56 in DTAB solution, giving an effective dielectric constant (ε_{eff}) of 26.0 for the SPA molecules microenvironment in DTAB micelles. In 0.02 M SDS solutions, $A_{max}/A_{min} = 4.51$ giving $\varepsilon_{eff} = 47.5$, and in 0.05 M SDS solutions, $A_{max}/A_{min} = 3.304$, giving $\varepsilon_{eff} = 31.5$.

The values of ε_{eff} indicate that SPA molecules are probably located in the Gouy–Chapman ionic layer of micelles. In DTAB micelles SPA molecules are closer to the micellar surface than in SDS micelles, because of the positive charge and increased hydrophobicity of the DTAB micelles surface. The dependence of ε_{eff} with concentration of SDS may indicate a partition equilibrium of SPA molecules between the aqueous intermicellar phase and the surface of the micellar pseudophase.

The observed interaction was similar to that found between acrylic acid and micelles [27], with interesting implications in emulsion polymerization [28].

References

1. Li S (1987) Youse Jinshu 39(10):18
2. Balachandian SR, Simkovich C, Arlan FF (1987) Int J Miner Process 21(3–4): 185
3. Braun H, Chichos Ch (1987) Abh Acad Wiss DDR, Abt Math Naturwiss Tech 1N:505
4. Kuys JK, Roberts NK (1987) Colloids & Surfaces 24:1
5. Dietze U, Braun J, Peter HJ (1987) Fresenius Z Anal Chem 322:17
6. Chichos Ch (1984) Tenside Deterg 21(2):1022
7. Ford DN, Braun ARA, Canada Patent C.A. 11591, 63 A1
8. Wottsen E (1980) Freiberg Forschungsch A (1980) A621:80
9. Rizkalla EN, Zaki MTM (1979) Talanta 26(10):979
10. Hurt V, Benicki M, Kacani S, Jozefcek J, Patent Czechoslovakia CS 120519
11. Elfers G, US Patent 232528
12. Mikroyannidis JA (1987) Phosphorus and Sulphur 32:113
13. Bergman E, Bondi A (1930) Ber Deutsch Chem Gesellschaft 63:1158
14. Vand V (1948) Acta Cryst 1:109
15. Vand V (1948) Acta Cryst 1:290
16. Davies CW (1962) Ion Association, Butterworths London, pp 41
17. Cardinal JR, Mukerjee P (1978) J Phys Chem 82:1614
18. Washburn EW Ed. (1928) International Critical Tables of Numerical Data Physics, Chemistry and Technology, McGraw Hill, New York
19. Mandel J (1964) Statistical Analysis of Experimental Data, Interscience Pub Co, New York
20. Schulz PC, Abramento M, Puig JF, Soltero-Marginez FA (1995) submitted
21. Schulz PC (1983) Anales Asoc Quim Argentina 71:271

22. Klose G, Petrov AG, Volk F, Meyer HW, Förster G, Rettig W (1982) Mol Cryst Liquid Cryst 88:109
23. Chapman D (1958) J Chem Soc 152:784
24. Kabachnik MI (1956) Doklady Akad Nauk SSSR 110(9):393
25. Schulz PC, Lelong ALM (1976) Rev Latinoamer Quim 7:9
26. Rizkalla EN, Zaki MTM (1979) Talanta 36:797
27. Corona-Galván S, Castañeda-Pérez J, Martínez-Gómez A, Puig JE, Schulz PC (1990) Colloid Polym Sci 268:778
28. Corona-Galván S, Castañeda-Pérez J, Schulz PC, Miller WG, Domínguez JM, Puig JE (1991) Polym Eng & Sci 31(6):409 – Puig JE, Corona-Galván S, Maldonado A, Schulz PC, Rodríguez BE, Kaler EW (1990) J Colloid Interface Sci 137:308